JOURNAL OF MATERIALS SCIENCE 20 (1985) 1141–1149

Thermal cycling of a unidirectional graphite–magnesium composite

E. G. WOLFF
The Aerospace Corporation, Materials Sciences Laboratory, El Segundo, California 90245, USA

B. K. MIN
Lockheed Palo Alto Research Laboratory, Palo Alto, California 94304, USA

M. H. KURAL
Lockheed Missiles and Space Company, Sunnyvale, California 94086 USA

Thermal cycling induced deformations of a unidirectionally reinforced graphite fibre–magnesium matrix composite are analysed with a micromechanical elastic–plastic model. The model is capable of describing the cyclic thermal behaviour as influenced by the matrix plasticity including strain hardening and Bauschinger effects. The analysis traces the entire thermal history over 18 cycles in the ± 100° C range. Predictions correlate well with measured strains, especially in terms of trends in the coefficient of thermal expansion. The results suggest further attention is required for time and temperature dependent stress relaxation rates and the role of defects.

1. Introduction

High specific strength, stiffness and thermal and electrical conductivities make graphite reinforced metals an attractive class of candidates for many structural applications. A near-zero coefficient of thermal expansion (CTE) is made possible in at least one direction by the use of high stiffness graphite fibres whose axial CTE values approach that of single crystal graphite in the "a" direction, namely $-1.62 \times 10^{-6}\ ^{\circ}C^{-1}$. However, the combination of stiff fibres with slightly negative CTE's and relatively compliant metals with high positive CTE's leads to large internal stresses in the constituents and plastic flow in the matrix after only slight temperature changes. While this behaviour does not necessarily reduce the mechanical properties of the composite, part of the total composite strain generated in the plastic loading cycle will be permanent. Repeated thermal or stress cycling will therefore lead to both instantaneous and cumulative dimensional instability.

This work is directed towards the measurement and prediction of thermal strains in a metal matrix composite, at least to the degree of accuracy attainable in essentially elastic composite systems (e.g. graphite epoxy in fibre dominated directions). This implies the use of measurement techniques capable of $\mu m\, m^{-1}$ resolution and accuracy. A mathematical model must consider constituent properties and geometry under combined mechanical and thermal loading. An immediate practical goal is the prediction and experimental verification of the temperature range where elastic behaviour predominates, for here the CTE is readily computed by classical lamination theory. The effective CTE during the plastic loading cycle and the net strain at the completion of a cycle are also of interest. The prior thermal history affects the stress state of the matrix and must therefore be included in the analysis.

2. Test sample

The unidirectionally reinforced graphite magnesium test rod was made of 42.5 volume % Pitch 100 (VS0054) fibres and an AZ91C alloy matrix by pultrusion of composite wires at Materials Concepts, Incorporated (Columbus, Ohio).

The thermal history begins with the stress–free

0022–2461/85 $03.00 + .12

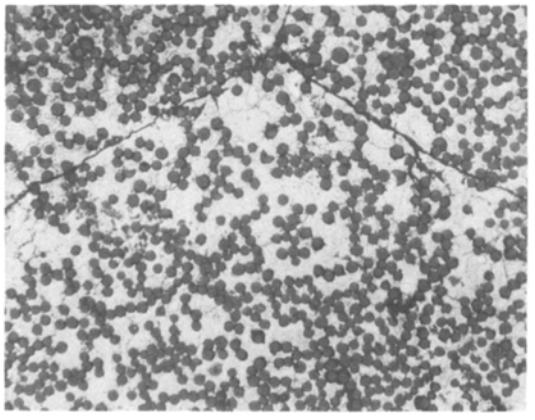

Figure 1 Microstructure of graphite–magnesium pultruded rod (× 200).

state of the composite system at the rod consolidation temperature of 468° C. The rod was air cooled and also chilled to 0° C, a condition believed to have happened during transportation according to test results. This state of the rod at room temperature is considered to be the reference condition for the material system.

Table I summarizes the constituent properties used for subsequent analysis. Fig. 1 illustrates the microstructure. Fibre distribution is fairly uniform and good bonding between fibre and matrix is apparent. Occasional axial cracks at the wire boundaries appear to have oxide layers 3–6 μm thick. The possibility of alloying element segregation at the fibre–matrix interface was investigated with an ion microprobe mass analyser (IMMA). The AZ91C is nominally Mg + (8–9% Al) + (0.4–1% Zn) + (0.13% minimum Mn). The compounds normally precipitating on heat treatment are δ-$Mg_{17}Al_{12}$ and $Mg_3Al_2Zn_3$. Mass spectral scans indicated uniform magnesium and hydrogen distribution, minimal silicon, and titanium and boron preferentially around the fibres. Fig. 2b shows the aluminium distribution (light areas) in a region shown in Fig. 2a. It is similar to the magnesium distribution. Figs. 2c and d were made at mass numbers of about 64 (TiO or Zn) and 48 (Ti or Mg_2), respectively. The difference between the two represents the zinc distribution. Scans at other locations indicate calcium, aluminium, titanium and chromium concentrated in cracks. The IMMA results therefore suggest some segregation occurred, resulting in a purer magnesium matrix than the AZ91C alloy.

TABLE I Material properties

Designation*	Fibre P100 (VS0054)	Matrix AZ91C-T4	Magnesium
E_{11} (GPa)	655	45.4	
E_{22} (GPa)	9.93	45.5	
ν_{12}	0.41	0.35	
G_{12} (GPa)	19.9	16.8	
$\alpha_1(\mu\epsilon\,^\circ C^{-1})$	−1.62	26.1	
$\alpha_2(\mu\epsilon\,^\circ C^{-1})$	21.6	26.1	

*E_{22} = transverse Young's modulus (in the fibre plane); G_{12} = in-plane shear modulus.

Mechanical properties of (hot pressed wire) VS0054/AZ91C samples with 3 mil (76 μm) AZ61A surface foils in the as-fabricated condition show rule of mixtures elastic moduli in the fibre direction at room temperature (about 290 GPa). This decreases to 241 GPa after 250 cycles in nitrogen between ± 125° C [1]. There is little effect of such cycling on the 150° C value (also about 241 GPa). The data (obtained with an extensometer) were taken on unloading. The stress–strain curve is essentially linear to failure in the fibre direction. More information on the matrix σ–ϵ characteristics could be obtained with transverse tensile tests but a thicker sample would be needed as the surface foils (about 25% of thickness) need to be machined off.

3. Experimental procedure

Fig. 3 illustrates the system used to measure $\Delta L/L$ as a function of temperature. The 0.289 m long graphite–magnesium rod was mounted on ULE* glass blocks with V-grooves to minimize motion relative to the helium–neon laser beams. The two arms of a Michelson interferometer reflect off ULE mirrors attached to the sample ends, which have been ground flat, parallel and perpendicular to the sample length axis. Initially, the mirrors were clamped in place, aligned optically and then bonded to the rod with ceramic cement or Varian Torr-Seal low outgassing epoxy adhesive. Problems of cement curing or shrinkage were overcome by using steel springs and nichrome wire clamps. Sample cooling was accomplished by uniformly distributing liquid nitrogen around a copper tube. Heating was done with Nichrome resistance wires in glass insulator tubes. One laser beam was phase modulated by a piezoelectric transducer (PZT) driven mirror and the resultant photodetector signals were analysed by comparing the harmonics in the fringe pattern

*"ULE" Ultra Low Expansion Glass, Code No 7971, Corning Glass Works, Corning, NY 14830.

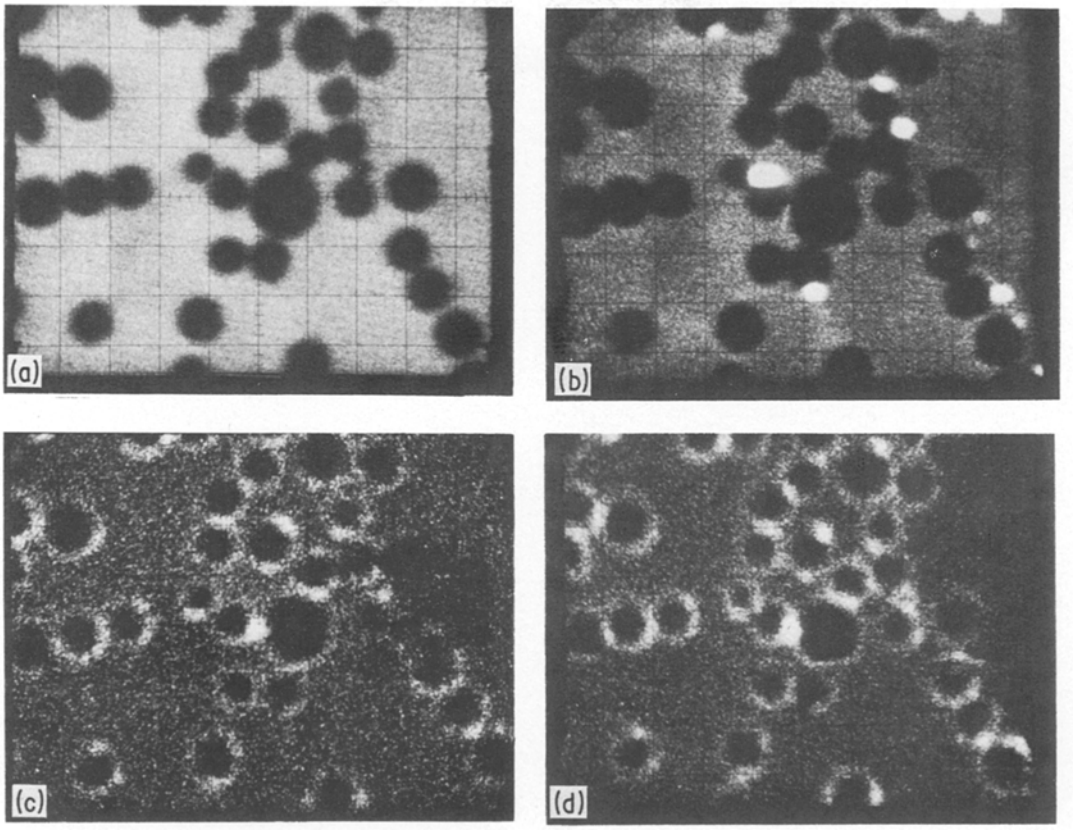

Figure 2 (a) Ion image for Mg^+ (m/e 25); (b) ion image for Al^+ (m/e 27); (c) ion image for m/e 64 ($TiO^+ + Zn^+$); (d) ion image for m/e 48 ($Ti^+ + Mg_2^+$).

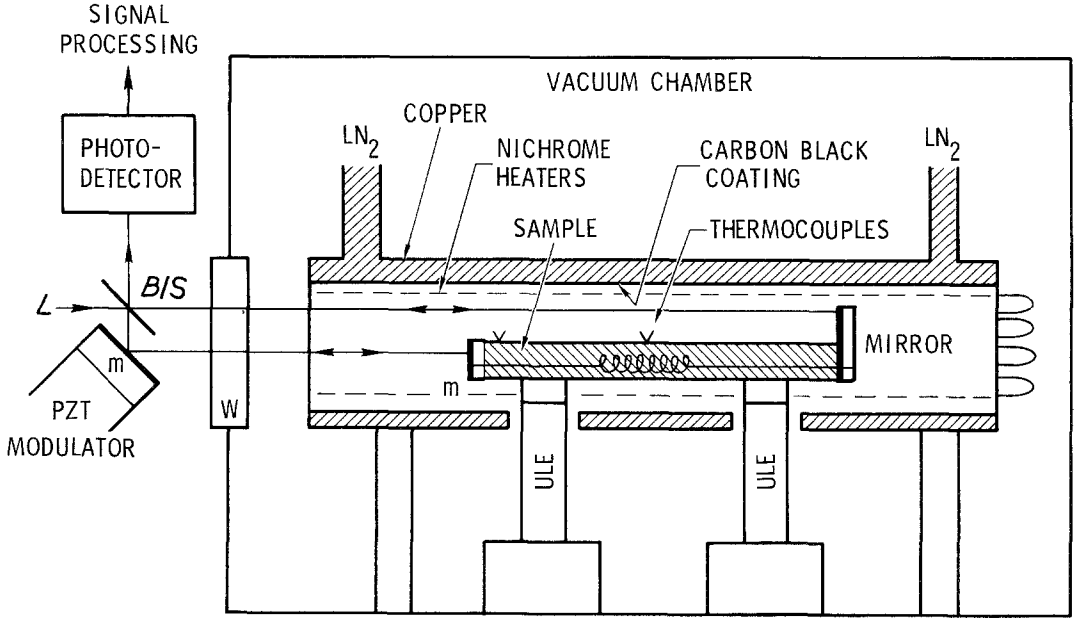

Figure 3 Schematic of thermal cycling apparatus and sample support.

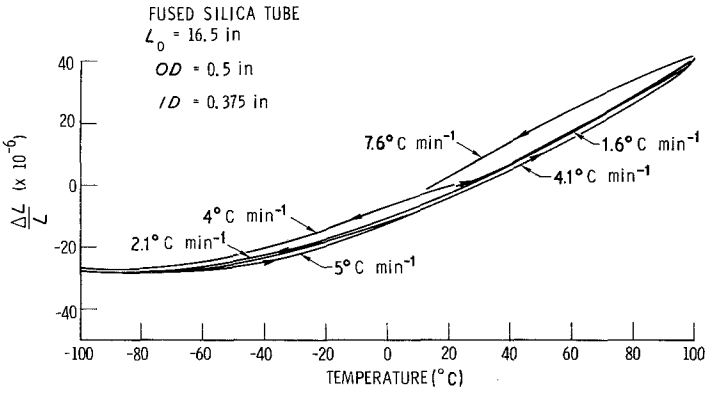

Figure 4 Calibration measurement of test apparatus using a silica tube 0.419 m long, 0.0127 m outside diameter, 0.0095 m inside diameter.

[2]. At least two copper–constantan thermocouples (0.05 mm diameter) were attached via Torr-Seal.

The method was tested with a 9.5 mm diameter quartz tube. Excellent agreement was obtained with the $\Delta L/L$ versus T curves obtained for a commercial fused quartz tube [3]. Fig. 4 shows the results of two such cycles. Differences were attributed to thermal lag effects. Due to higher thermal conductivity, the graphite–magnesium tube could be expected to exhibit transverse temperature gradients of $< 1^\circ$ C at heating rates of $\leqslant 2^\circ$ C min^{-1}. Maximum longitudinal gradients were found to be 1.1° C at 100° C and 0.4° C at -60° C. Purely vertical or horizontal movements of the sample would not produce an error. Use of short focal length lenses reduces the incidence of lost signals but introduces possible errors due to unknown index of refraction gradients on heating or cooling.

The initial optics supports were sensitive to room temperature fluctuations and showed equivalent random excursions of about $\pm 2\,\mu\varepsilon$. After the sixth cycle the optics were mounted on Invar supports and the air path of the beams minimized. Fig. 5 includes isothermal data for the quartz calibration runs No. 3 (heated to 99° C at 3.1° C min^{-1}) and No. 4 (4.0° C min^{-1}). At 99° C it is seen that the more rapidly heated sample continues to expand with time as its average temperature increases. The system stability at the temperature extreme is within $\pm\ 1\,\mu\varepsilon$ for at least 100 min. Cooling rates decrease below 2° C min^{-1} at $\leqslant 60^\circ$ C due to slower radiation heat transfer. The stability data here suggest less than $\pm 0.5\,\mu\varepsilon\,h^{-1}$ drift after an initial 30–40 min. The rod was subjected to eighteen thermal cycles, of which most consisted of 22° C to 100° C to T_3 to 22° C, where T_3 varied from -19° C to -99° C. Cycles 4, 6 and 16 involved cooling first, then heating. Cooling or heating rates were generally 1 to 2° C min^{-1}. Isothermal holds at 99 and -99° C were carried out in Runs 14 and 17. Fig. 5 shows the resultant creep due to internal stress relaxation. The hold at -99° C in Run 17 showed considerable strain scatter, suggesting discontinuous ΔL's. The scatter for Run 14 at -99° C (not shown) was similar.

4. Analysis

The thermal expansion behaviour of the graphite–magnesium rod was analytically examined with the use of the "mechanics of materials" model [4–6], particularly developed for the elastoplastic thermal expansion analysis of continuous fibre metal matrix composites. In this model, the stresses and strains of the fibre and matrix are assumed to be uniform satisfying the plane stress kinematic relationship

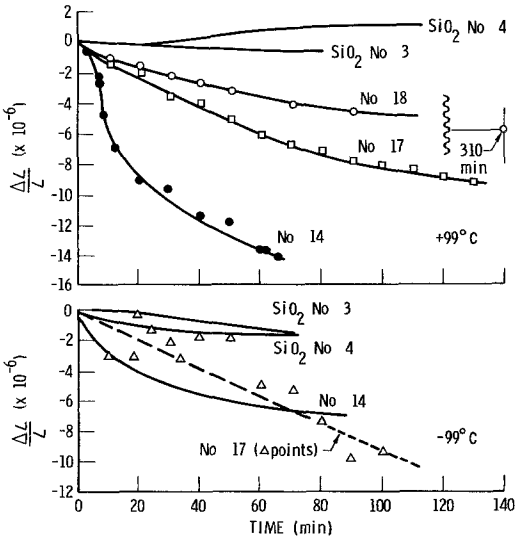

Figure 5 Creep data at $+99$ and -99° C for silica calibration tube (Tests No 3 and 4) and the graphite–magnesium rod (during cycles 14, 17 and 18).

represented by

$$\sigma_1 = \nu_f \sigma_1^f + \nu_m \sigma_1^m$$
$$\sigma_2 = \sigma_2^f = \sigma_2^m \quad (1)$$
$$\tau_{12} = \tau_{12}^f = \tau_{12}^m ,$$
$$\epsilon_1 = \epsilon_1^f = \epsilon_1^m$$
$$\epsilon_2 = \nu_f \epsilon_2^f + \nu_m \epsilon_2^m \quad (2)$$
$$\gamma_{12} = \nu_f \gamma_{12}^f + \nu_m \gamma_{12}^m .$$

where ν_f and ν_m are the volume fractions of the fibre and matrix, respectively. σ denotes normal stress; ϵ, normal strain; τ, shear stress; and γ, engineering shear strain. The superscripts, f and m, denote the fibre and matrix, respectively; the stresses and strains with no superscript denote those of the composite. The coordinates 1 and 2 are parallel and perpendicular, respectively, to the direction of fibres.

The elastic constants and the coefficients of thermal expansion for the unidirectional composites consisting of isotropic fibre and matrix have been derived based on the above kinematic relations [7]. The corresponding thermoelastic properties for general unidirectional composites where the fibre and matrix are both orthotropic linear elastic materials have been derived in [5, 6]. In the present analysis model, the fibre is assumed to be orthotropic linear elastic material and the matrix to be isotropic elastic–plastic material. The fibre strain is assumed to consist of elastic and thermal parts: and the matrix strain to consist of elastic, plastic and thermal parts which are additive to each other.

The elastic–plastic behaviour of the matrix is described by the White–Besseling model [8, 9] also known as the mechanical sublayer model. The White–Besseling model is particularly suitable for describing the cyclic elastic–plastic behaviour of metals including the strain hardening and Bauschinger effects. In the present work, the White–Besseling plasticity formulation is implemented by adapting the numerical procedure of Hunsaker *et al.* [10] to the case of plane stress.

A full discussion on the properties and numerical implementation of the present analysis model is beyond the scope of this paper; the reader may refer to Min and Flaggs [6] for details. The longitudinal thermal expansion behaviour of the graphite–magnesium rod was analysed using this model implemented by the advanced laminate analysis (ADVLAM) code [11]. Implicitly assumed in the analysis is the absence of externally applied mechanical loading in which case the longitudinal thermal expansion behaviour of a rod is identical to that of a unidirectional lamina.

5. Results

The analysis was performed using an incremental technique to trace the temperature history of the graphite–magnesium rod. Fig. 6 shows the predicted thermal expansion behaviour of the graphite–magnesium rod for all eighteen cycles. As mentioned before, the reference or the zero strain condition was taken to be the state of the rod at room temperature following an excursion to 0° C after the cool down from the manufacturing temperature. All subsequent rod strains were adjusted to this reference state as if the cycling process were continuous for eighteen cycles.

It can be seen from Fig. 6 that the rod experiences a total strain of approximately 200 μm m^{-1} during this cycling process. The strain within the ± 100° C cycling temperature range translates into an effective CTE of ~ 1 $\mu\epsilon$ ° C^{-1}. The CTE of the rod also exhibits positive and negative values during thermal cycling indicating its dependence on the elastic and plastic state of the matrix material. The maximum positive CTE is attained during the heating cycles with a value of approximately 0.7 $\mu\epsilon$ ° C^{-1}. This CTE is associated with the elastic behaviour of the matrix during the unloading process. The minimum value of CTE during cooling cycles is approximately − 1.5 $\mu\epsilon$ ° C^{-1} which is very near to the fibre CTE of − 1.62 $\mu\epsilon$ ° C^{-1}, indicating near perfect plasticity for the matrix material.

The behaviour of the matrix is plotted in Fig. 7 in terms of matrix stresses and strains. Note that the plot covers the total thermal history of the rod from the stress-free state at consolidation to the end

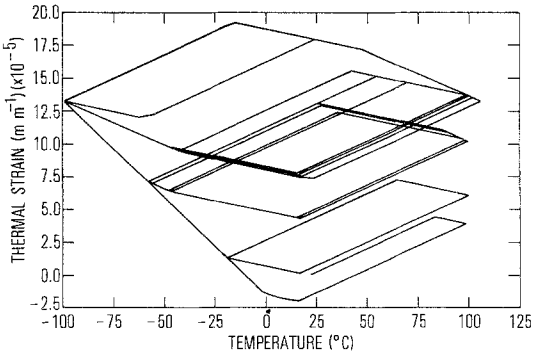

Figure 6 Predicted thermal strain versus temperature of the graphite–magnesium rod for 18 thermal cycles.

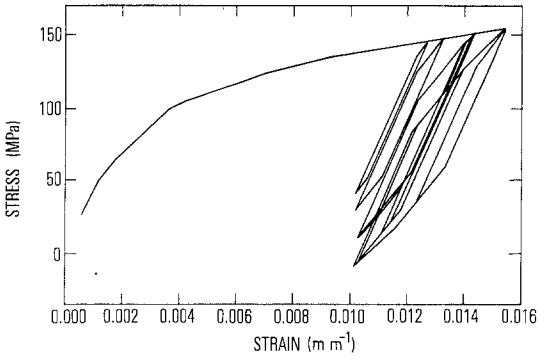

Figure 7 Stress–strain behaviour of the graphite–magnesium rod matrix for 18 thermal cycles.

of the eighteenth cycle. Following this diagram, it is seen that the matrix material has yielded considerably during the first cool down from the manufacturing temperature to the baseline state at room temperature. During subsequent heating, the matrix unloads until the onset of reverse yielding. The next cooling phase once again makes the matrix material behave elastically until yielding occurs. Further cooling forces the material to follow the original stress–strain curve at which region the rate of plastic flow is near maximum. The behaviour of the matrix material for the remaining cycles is similar except that the hysteresis loops tend to move toward higher strain values as the rod is exposed to cooler temperatures.

Figs. 8 to 13 show both the measured thermal strains and the predicted strains for the first six cycles. Each cycle is totally dependent on the history of the previous cycles, including the stress-free state at consolidation. These results correlate well with the predicted expansion curves, especially in terms of CTE trends. For example, the calculated expansion behaviour of the rod shown in Fig. 8

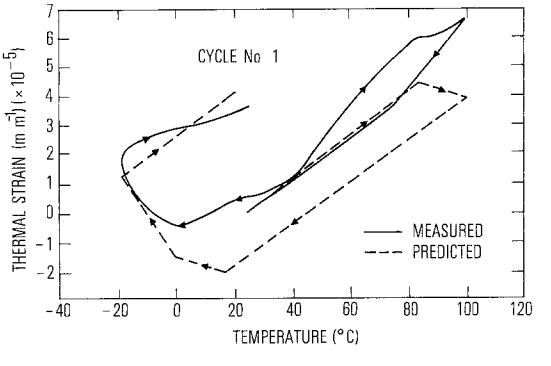

Figure 8 Measured and predicted (dashed lines) thermal strain versus temperature for the graphite–magnesium rod subjected to thermal cycle 1 (22 to 99 to −19 to 22° C).

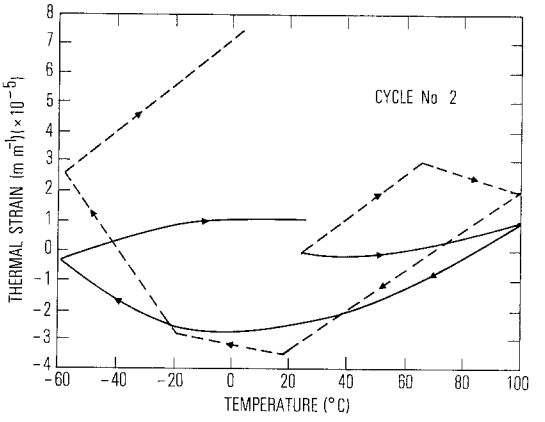

Figure 9 Data for thermal cycle 2 (22 to 100 to −58 to 22° C).

representing the first cycle is very similar to the overall experimental trend. In terms of absolute values, slopes representing the elastic and plastic coefficients of thermal expansion also correlate well. The calculated elastic value of the CTE during the first heating and cooling phase is 0.73 $\mu\varepsilon\,^{\circ}\,C^{-1}$ and approximately 0.9 $\mu\varepsilon\,^{\circ}\,C^{-1}$ for the measurement. Similarly, cooling to −19° C gives 1.5 and 2 $\mu\varepsilon\,^{\circ}\,C^{-1}$ for the predicted and the experimental CTE values. Comparison of other cycles also shows remarkable expansion behaviour similarities between test results and values obtained by analysis.

Fig. 5 shows that various creep rates occur at the temperature extremes, presumably due to internal stress relaxation. This suggested that creep may influence the results at all temperatures, including holds between cycles. Listed data from other cycles substantiated this view. When the sample has been cooled sufficiently, (e.g. in Cycle 2), the theory predicted that continued heating should exhibit a

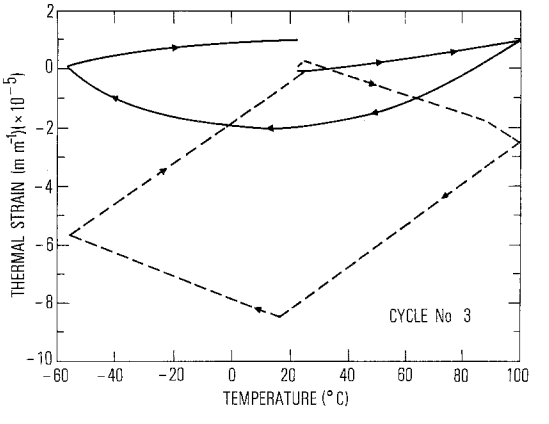

Figure 10 Data for thermal cycle 3 (22 to 99 to −56 to 22° C).

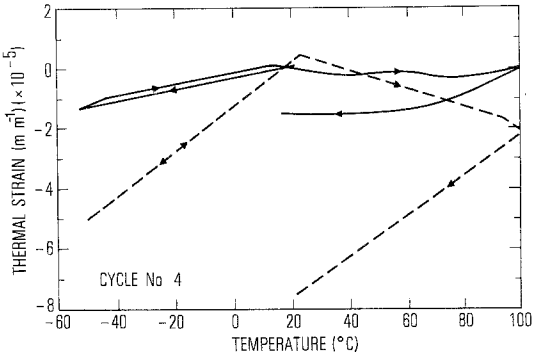

Figure 11 Data for thermal cycle 4 (22 to −52 to 99 to 22° C).

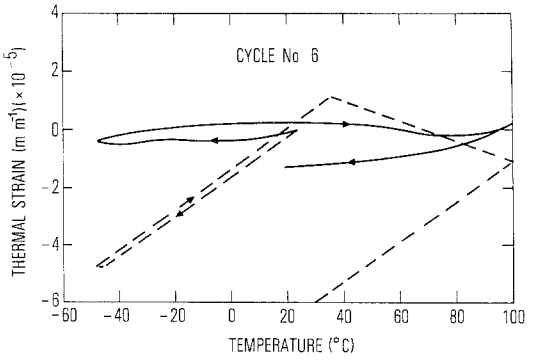

Figure 13 Data for thermal cycle 6 (23 to −48 to 100 to 22° C).

negative CTE. This indeed was found when the next cycle (e.g. Cycle 3 to 100° C) began within a few hours after the previous one. However, in one case there was a 5 day hold at 23° C (between cycles 7 and 8). This evidently allowed considerable stress relief from the prior heating from −97° C. Consequently, elastic behaviour (with a positive CTE) was measured at the start of cycle 8.

6. Discussion

The measurement of thermal strain hysteresis of metal matrix composites in fibre dominated directions requires real time strain sensitivity on the order of 10^{-6} m m^{-1}. This was achieved with Michelson laser interferometry and phase modulated signal processing. The accuracy of the method was verified by tests on quartz rods of similar dimensions as the test sample. Further improvements are needed for the measurement of attendant isothermal creep phenomena e.g., to 1 μm m^{-1} 100 h^{-1}. Elimination of the air paths in the interferometer by moving the beam splitter and modulating mirror into the vacuum chamber would be helpful.

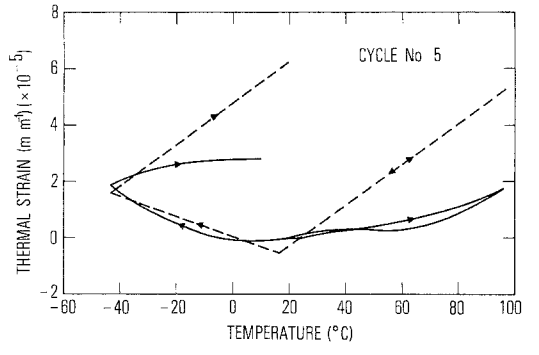

Figure 12 Data for thermal cycle 5 (24 to 96 to −46 to 24° C).

The results suggest that alloying elements and impurities segregate at the fibre–matrix interface and at imperfections such as cracks. Correlation of creep data with matrix properties would need further examination of these phenomena. For example, the presence of coatings, impurities and alloying constituents at the fibre–matrix interfaces should be influenced by fibre type and pretreatment. Since oxides are normally found on graphite fibre surfaces one would expect the most stable oxide in the system (in this case MgO) to be present there preferentially with attendant depletion of the metallic element in the matrix. Changes in the matrix composition might be monitored by a combination of microhardness and electrical conductivity measurements [12]. Ageing effects, possibly modified by segregation, were reported for AZ91C-T4 near room temperature [13]. Contraction at $T < 100°$ C is followed by expansion after long times. This occurs sooner as the temperature is raised above 100° C.

The present results show that the temperature range of elastic behaviour may be quite small, e.g. less than 100° C. In addition, the type of behaviour depends on prior history and the degree of internal stress modification. The discovery of creep effects here at all temperatures within the measurement range suggests that the thermal strains are rate dependent. Further work is called for to determine the effect of matrix creep behaviour.

The analytical model considers the influence of matrix plasticity during cyclical thermal behaviour and includes work hardening and Bauschinger effects. The major discrepancy between predicted and measured values lies in the magnitude of the predicted expansion when elastic behaviour is expected (e.g., after unloading from plastic deformation). This could be accounted for by almost continual creep as a form of stress relief during

thermal cycling. It may also be influenced by the axial cracks which may reduce shear coupling and generate small Poisson's effects, and/or by the time and temperature dependence of the matrix σ–ϵ relations. The latter phenomena, i.e., nonisothermal plasticity and creep, are primary candidates for further reinforcement of the present analysis model.

In practice, the effective average CTE over a wide temperature range is of frequent interest. These results indicate that high modulus graphite fibres in low modulus metal matrices can maintain CTE's of less than $1 \times 10^{-6}\,^{\circ}C^{-1}$ over the $\pm 100^{\circ}$ C range. On the other hand, control of dimensions to $< 10^{-5}\,m\,m^{-1}$ is hampered by time dependence, irreproducibility, net dimensional changes and possibly matrix compositional changes during thermal cycling, at least for 18 cycles in the $\pm 100^{\circ}$ C range. Since plasticity of the matrix is the major cause of the thermal hysteresis, control of matrix properties, e.g., through heat treatment or alloying, is a primary candidate for control of the dimensional changes.

7. Summary and conclusions

The thermal expansion behaviour of a unidirectionally reinforced graphite–magnesium rod was studied over eighteen cycles between $\pm 100^{\circ}$ C by experimental measurements and theoretical modelling. Since this material possesses a near zero CTE in the fibre direction, a high resolution ($\pm 1\,\mu\epsilon$) laser Michelson interferometer was employed to monitor the thermal response. Prior characterization of the rod with an ion microprobe analyser suggested that segregation during fabrication resulted in a purer magnesium matrix than the nominal AZ91C alloy.

The experimental results showed that the thermal expansion of graphite–magnesium exhibits complex behaviour including nonlinearity, history and time dependence, and hysteresis loops during thermal cycling. Isothermal creep strains at $\pm 99^{\circ}$ C are asymptotic to 5 to 20 $\mu\epsilon$ at times over an hour.

A micromechanical model was employed to analyse the nonlinear and hysteresis behaviour. The model considers "mechanics of materials" type of interactions between the fibre and matrix, and the plasticity of the matrix including strain hardening and Bauschinger effects. The correlation between theory and experiment is remarkably good in terms of hysteresis trends, especially when the complexity of the problem is considered. Discrepancies are attributed mainly to the continual creep of the matrix during thermal cycling and the temperature dependence of the matrix yield strength, which were not covered by the analysis. Longitudinal cracking in the matrix and/or the oversimplification of the fibre–matrix model employed in the present analysis may be responsible for an additional part of the discrepancy.

Automated heating and cooling rates and continuous strain monitoring of the sample between cycles are recommended as experimental improvements for further studies of graphite–metal matrix systems. The creep and nonisothermal plasticity effects are the prime candidates to be included in the analytical model to improve the accuracy of the predictions of strain–temperature–time behaviour.

Acknowledgements

This work was performed under the Aerospace Mission Oriented Investigation and Experimentation Program and the Lockheed Independent Research and Development Programs. The authors wish to thank W. H. Dittrich and R. Savedra for assistance with the dimensional measurements and N. Marquez for the IMMA analysis.

References

1. Dr. G. STECKEL, Aerospace Corp, private communication.
2. S. A. ESELUN, R. C. SAVEDRA and E. G. WOLFF, Report SD-TR-81-113 (Space Division AFSC), 18 December (1981).
3. E. G. WOLFF and S. A. ESELUN, *Rev. Sci. Instr.* **50** (1979) 502.
4. B. K. MIN, *Mech. Phys. Solids,* **29** (1981) 327.
5. B. K. MIN and F. W. CROSSMAN, in Proceedings of the 6th Conference on Composite Materials: Testing and Design, ASTM STP 787, edited by I. M. Daniel (American Society for Testing and Materials, 1982) p 371.
6. B. K. MIN and D. L. FLAGGS, to be published in Proceedings of ASME Conference on Pressure Vessels and Piping, New Orleans, June 1985.
7. S. W. TSAI and H. T. HAHN, "Introduction to Composite Materials," (Technomic Publishing Company, Westport, Connecticut, 1980) p. 389.
8. G. N. WHITE, Jr., "Application of the Theory of Perfectly Plastic Solids to Stress Analysis of Strain Hardening Solids," Brown University, Technical Report **51** (1951).
9. J. F. BESSELING, "A Theory of Plastic Flow for Anisotropic Hardening in Plastic Deformation of an Initially Isotropic Material," Report S410 (National Aeronautical Research Institute, Amsterdam, The Netherlands, 1953).
10. B. HUNSAKER, Jr., D. K. VAUGHAN, J. A. STRICKLIN and W. E. HAISLER, "A Comparison of Current Work-Hardening Models Used in the

Analysis of Plastic Deformation," TEES-RPT-2926-73-3, October 1973 (Aerospace Engineering Department, Texas A & M University, College Station, Texas).
11. D. L. FLAGGS, "ADVLAM – An Advanced Composite Laminate Analysis Code" (Lockheed Missiles and Space Company, 1982).
12. R. A. CHIHOSKI, *Met. Prog.*, **123** (1983) 27.
13. "Metals Handbook", edited by T. Lyman, 8th Edition, **2** (1964) Fig. 4, p. 269.

Received 13 December 1983
and accepted 12 April 1984